PATHOLOGICA 2025;117:278-287**;**
DOI: 10.32074/1591-951X-939

Original article

Histological and proteomic characterization of musculoskeletal amyloidomas

Raffaele Gaeta[1*], Francesco Greco[2,3*], Federica Anastasi[2,4] Lorenzo Andreani[5], Rodolfo Capanna[5], Liam A. McDonnell[2], Alessandro Franchi[6]

[1] Division of Surgical Pathology, University of Pisa, Pisa, Italy; [2] Fondazione Pisana per la Scienza ONLUS, San Giuliano Terme (PI), Italy; [3] Institute of Life Sciences, Sant'Anna School of Advanced Studies, Pisa, Italy; [4] NEST Laboratories, Scuola Normale Superiore, Pisa, Italy; [5] Department of Orthopaedic and Trauma Surgery, University of Pisa, Pisa, Italy; [6] Department of Translational Research and of New Technologies in Medicine and Surgery, University of Pisa, Italy

**These authors contributed equally to the study*

Summary

Introduction. The term amyloidoma applies to localized deposits of amyloid in the absence of systemic amyloidosis. Skeletal and soft tissue amyloidomas are very rare and the pathogenesis is usually associated with lymphoproliferative disorders (plasmacytomas or plasmacytoid lymphomas) or as a consequence of local chronic inflammation.

Methods. In this paper we report the histological and immunohistochemical features of four cases of musculoskeletal amyloidoma in association with combined laser capture microdissection (LCM) of Congo Red positive regions with a recent microproteomics workflow that improves the sensitivity of the analysis in order to confirm the nature of the protein deposit.

Results. Proteomic techniques allowed to elucidate the nature of the amyloid protein deposit, improving the results obtained by immunohistochemistry (IHC). IHC results were confirmed in two cases while LCM coupled with bottom-up microproteomics was necessary to type the other two cases, for which IHC was inconclusive.

Conclusions. In conclusion, proteomic techniques were thus confirmed as a fundamental tool for the complete investigation of protein deposits.

Key words: amyloidoma, proteomics, immunohistochemistry, LC-MS/MS, histology

Received: October 23, 2024
Accepted: November 13, 2024

Correspondence
Raffaele Gaeta
E-mail: raffaele.gaeta@med.unipi.it

How to cite this article: Gaeta R, Greco F, Anastasi F,, et al. Histological and proteomic characterization of musculoskeletal amyloidomas. Pathologica 2025;117:278-287; https://doi. org/10.32074/1591-951X-939

Introduction

The term amyloidoma applies to localized deposits of amyloid in the absence of systemic amyloidosis. Amyloidomas affecting the skeleton and the soft tissues are very rare and the clinical presentation as mass lesions frequently leads to the initial suspicion of a neoplasm. Bone involvement occurs more frequently in the axial skeleton, mainly in the thoracic spine and skull [1], while soft tissue amyloidomas localize more frequently in the mediastinum and retroperitoneum, as well as in the extremities [2]. Regarding their pathogenesis, bone and soft tissue amyloidomas of the mediastinum or abdomen are frequently associated with lymphoproliferative disorders (plasmacytomas or plasmacytoid lymphomas), whereas soft tissue amyloidomas of the extremities may arise as a consequence of local chronic inflammation [1,2]. The histopathologic diagnosis requires the identification and characterization of the amyloid, and this may be difficult because amyloid deposits may be obscured by

inflammation and giant cell foreign body reaction or may undergo calcification, bony metaplasia or present unusual morphology, including the formation of corpora amylacea-like structures with concentric lamination. Antibody-based techniques for amyloid typing are widely used in clinical practice [3]. However these techniques have some limitations, linked to the non-specificity of the antibodies to the mutated or truncated forms of amyloid proteins and with the non-specific interactions of the antibody with fibrils [4]. In the last decade mass spectrometry based bottom-up proteomics, along with electron microscopy, has become one of the reference techniques for amyloid typing [4,5] and several protocols have been developed [6-8]. Bottom-up proteomics is based on the proteolytic digestion of proteins and on the separation and analysis of the resulting proteolytic peptides by liquid chromatography coupled with tandem mass spectrometry (LC-MS/MS) [9,10]. Peptides are identified by matching their MS/MS spectra to in-silico simulated peptide spectra calculated from curated protein databases. The identified peptides are then merged to provide information at the protein level, both in terms of identity and quantity [11,12]. Proteomics can be coupled with laser capture microdissection (LCM) of Congo Red (CR) stained sections to focus the analysis on amyloid-containing regions [6]. LCM enables the precise dissection of specific tissue regions under a microscope, to isolate these regions-of-interest, and thereby to process them for proteomics analysis using liquid-based protocols [13]. Here we report the clinico-pathologic features of 4 cases of musculo-skeletal amyloidoma that were studied by combined LCM of CR-positive regions with a recently reported microproteomics workflow [14] that further improves the sensitivity of the analysis.

Patients and methods

Patients

The salient clinical features of the 4 cases of musculoskeletal amyloidoma analyzed in this study are summarized in Table I.

Materials

Histology-grade solvents and Congo Red were purchased from DiaPath S.p.A. (Martinengo, Italy). SuperFrost Plus glass microscope slides were purchased from VWR International, LLC (Radnor, PA, USA). LC-MS grade water, acetonitrile (ACN) and formic acid (FA) were purchased from Thermo Fisher Scientific (Rockford, IL, USA). Phosphoric acid was purchased from Merck (Darmstadt, Germany). Adhesive Cap 200

Table I. Summary of clinical data, proteomics analysis, immunohistochemical findings and histopathologic diagnosis of the 4 patients.

Case	Sex, Age	Site	Clinical background	Treatment	Abundant protein	Tentative MS-based diagnosis	Immunohistochemical findings	Histopathologic diagnosis
1	F 62	Soft tissues, leg	Sjogren syndrome, chronic liver disease	Intralesional resection	IGLV6-57	AL-λ chains	CD68+, MDM2-, CD138-, kappa-, lambda-	Soft tissue amyloidoma
2	F 83	Proximal femur and diaphysis	Multiple myeloma (monoclonal for Kappa chain)	Resection of proximal femur, prosthesis	IGKC	AL-k chains	MUM1+, CD138+, kappa+, lambda-, CD68-	Amyloidoma in multiple myeloma (kappa chain monoclonal)
3	M 58	Proximal femur	Multiple myeloma (monoclonal for Kappa chain)	Resection of proximal femur, prosthesis	IGKC	AL-k chains	kappa+, lambda-	Amyloidoma in multiple myeloma (kappa chain monoclonal)
4	F 65	Soft tissues, popliteal fossa	Type II diabetes mellitus; hypertension; no evidence of chronic inflammatory diseases or plasma cell proliferative disorders	Intralesional resection	IGKC	AL-k chains	CD68+, CD138+, kappa+, lambda+	Soft tissue amyloidoma

tubes were obtained from Zeiss (Oberkochen, Germany). All the other reagents were purchased from Sigma-Aldrich (Saint Louis, MO, USA).

Immunohistochemistry

Immunohistochemical analysis was conducted on formalin-fixed paraffin-embedded (FFPE) full tumor tissue sections. Five mm sections were deparaffinized, hydrated and after endogenous peroxidase inactivation, immunostained with BenchMark® Ultra stainer (Ventana, Tucson, AZ, USA). The following primary antibodies were employed: CD68 (clone KP1, Roche Diagnostics, Rotkreuz, Switzerland); kappa and lambda light chain (polyclonal, Roche Diagnostics, Rotkreuz, Switzerland); MDM2 (clone IF2, Invitrogen, Rockford, IL, USA); CD138/syndecan-1 (clone B-A38, Cell Marque, Darmstadt, Germany); MUM1 (clone EP190, Cell Marque, Darmstadt, Germany). The reaction was revealed with iVIEW DAB detection kit, providing a brown reaction product. After completing the staining process, the slides were removed from the autostainer, counterstained with hematoxylin, dehydrated and mounted with a permanent medium. As negative control, we substituted primary antibody with a Ventana dispenser filled with non-immune serum at the same concentration for each immunohistochemical reaction.

Laser capture microdissection

Tissue sections, 8 µm thickness, were cut using a Leica RM2245 microtome (Leica, Wetzlar, Germany) and mounted onto microscope slides using a Leica HI 1210 water warm bath (Leica). The tissue sections were heated at 60°C for one hour to increase adherence, then submerged in xylene twice for 15 minutes to remove paraffin, and finally stained with hematoxylin followed by Congo Red. The stained tissue sections were then mounted onto a Zeiss Axio Observer Z1 microscope equipped with a PALM Microbeam laser and a RoboMover (both Zeiss, Oberkochen, Germany) for LCM. Amyloid areas were detected in fluorescence mode (HPX 120C lamp, 43 DSRed filter, Zeiss) and confirmed under brightfield using the PALMRobo software (v 4.9, Zeiss). The microdissection laser was operated in AutoLPC mode, with a distance between spots of 10 µm and a distance from the border of 5 µm. Fragments were collected in the cap of Adhesive Cap tubes and stored at -20°C. The plaque from one sample (case 3) was manually collected from the glass slide using the tip of a pipette, since the tissue was fragile and detached from the slide. The average area isolated by LCM for each sample was approximately 0.25 mm^2.

Proteomics sample preparation

The lysis buffer, 35 µL of 10 mM Tris/ 1mM EDTA/5% SDS, was added to the tube caps containing the small pieces of tissue isolated by LCM. Blank samples were processed alongside the samples by adding the lysis buffer to empty Adhesive Cap tubes. Solutions were transferred to a clean tube. The tissue and solvent solutions were heated to 98°C for 90 min with occasional vortexing to effect heat-aided antigen retrieval. Samples were then sonicated using a Bioruptor Pico (Diagenode, Liège, Belgium) to lyse the tissues (15 cycles, 30 sec ON, 30 sec OFF), followed by heating to 95°C for 10 min. Proteins were reduced with dithiothreitol (final concentration 20 mM) and incubated at 45°C for 30 min. Protein alkylation was performed with iodoacetamide (IAA, final concentration 40mM) for 30 min at RT in the dark. Excess IAA was quenched by addition of another aliquot of DTT (final concentration 40mM). Proteins were then digested using Micro S-traps (ProtiFI, Farmingdale, NY, USA) as follows: A ratio of 1:10 v/v of 12% phosphoric acid was added to each sample, followed by 400 µL of S-trap binding buffer (90% MeOH, final TEAB concentration of 100 mM, pH 7.1). The protein extracts of the LCM samples were loaded on the S-trap columns and centrifuged at 4000xg for 1 min and the flow-through discarded. Multiple centrifugations were performed to load all the protein extract onto the S-trap column. Bound proteins were washed four times with 150 µL of S-trap binding buffer. Digestion was performed by loading 0.5 µg of trypsin/LysC (Promega, Madison, WI, USA) in 20 µL of digestion buffer (50 mM TEAB, pH 8) and incubating at 37°C for 18 hours. Peptides were eluted in three steps with 40 µL of 50 mM TEAB, 40 µL 0.2% FA and 35 µL of 50% ACN, each followed by a centrifugation at 4000xg for 1 min. Peptides were dried and resuspended in 10% formic acid and stored at -20°C until LC-MS/MS analysis.

Proteomics analysis

One tenth of the peptide amount was loaded onto an EASY-nLC 1000 (Thermo Scientific) equipped with an Acclaim PepMap 100 pre-column (2 cm x 75 µm, C18, 3 µm, 100 Å; Thermo Scientific). Peptides were separated with a 60 min gradient on an EASY-Spray analytical column (ES803: 50 cm x 75 µm, C18, 2 µm, 100 Å; Thermo Scientific) and analyzed using an Orbitrap Fusion Tribrid mass spectrometer (Thermo Scientific, San Diego, USA).

Peptide ions were analyzed using the Top Speed data dependent method, with a 3 sec cycle time; MS1 scans were performed in the Orbitrap (*m/z* 375 to 1500 at 120K resolution with an AGC Target $5x10^5$ and 100 msec maximum injection time) and MS2 scans

acquired in the ion trap using a 1.6 *m/z* isolation window, 30% HCD Collision Energy and an AGC target of $5x10^3$.

Raw data were analyzed using Proteome Discoverer (v.2.1, Thermo Scientific) and searched against the SwissProt *Homo sapiens* database (Uniprot, 21/10/2019, 20365 entries). An in-house contaminant database was added to the search (250 entries). Searches were performed with a precursor mass tolerance of 10 ppm and using a strict FDR of 0.01. A maximum of two missed cleavages were allowed. Methionine oxidation (+15.995 Da) and acetylation (+42.01 Da, protein N-terminus) were set as dynamic modifications while carbamidomethylation of cysteine (+57.021 Da) was set as a static modification. Protein Groups were filtered by eliminating protein identified in the contaminant database and precursor ion intensities were exported to GraphPad Prism for bar chart plotting (version 5, GraphPad Softwares, Inc, San Diego, CA). An online tool [15] was used to compare the Protein Groups between case 1 and 2. Enrichment analysis was performed in String [16] (v11.5) using the whole *Homo sapiens* database as background.

Results

Histopathologic findings

Two lesions (cases 2 and 3) presented with the usual histological appearance of amyloidoma and consisted of diffuse depositions of amorphous eosinophilic material, with focal giant cell reaction and with a sparse focal lymphoplasmacytic infiltrate (Fig. 1B). The deposits within the medullary bone were well circumscribed and surrounded by thickened trabeculae (Fig. 1A). In both cases, a uniform population of mature appearing plasma cells was present between the amyloid deposits. These were positive for immunohistochemical staining of kappa light chain and negative for lambda light chain.

In case 2 amyloid was deposited over the bony trabeculae, sometimes surrounding them, and undergoing mineralization as well as osseous metaplasia (Fig. 2A). In other areas amyloid deposits consisted in part of rounded structures reminiscent of corpora amylacea, which frequently displayed a concentric lamination and partial calcification (Fig. 2B).

In case 1 and 4, the soft tissue lesion consisted of lobules of mature adipose tissue separated by collagenous septa and by amorphous eosinophilic extracellular matrix. This was present in small amounts among adipocytes or accumulated in bands or large deposits without intervening adipocytic ele-

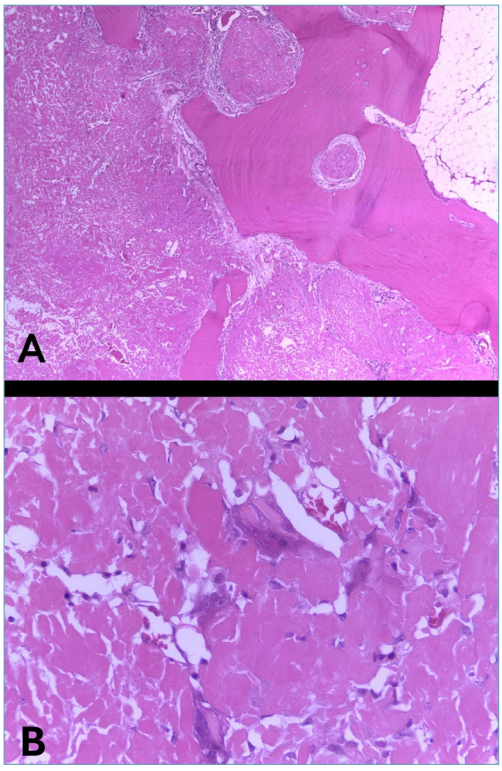

Figure 1. Amyloidoma of bone. The medullary spaces are occupied by deposits of amyloid substance, with marked thickening of bony trabeculae (A) (H&E, 2.5X). Foreign body-type multinucleated giant cells are detected within the amyloid (B) (H&E, 20X).

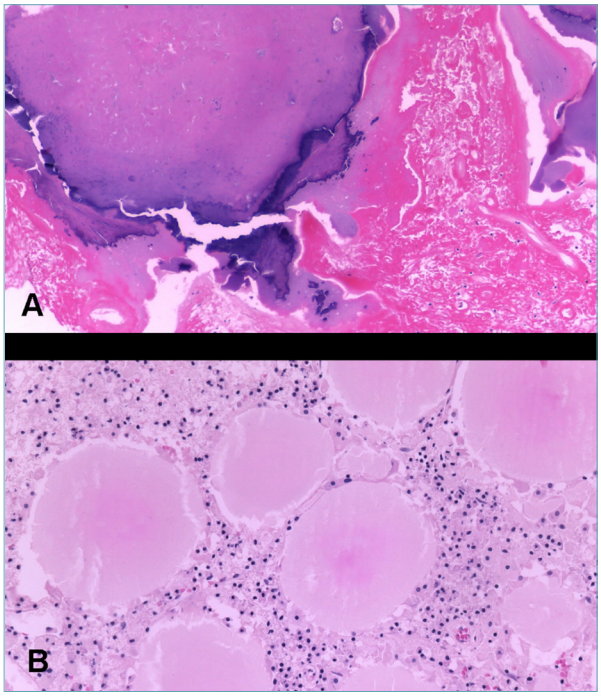

Figure 2. Amyloidoma of bone. In this case the amyloid appears both as amorphous eosinophilic and calcified masses (A) (H&E, 2,5X). In other areas, amyloid deposits present as rounded structures reminiscent of corpora amylacea (B) (H&E, 4X).

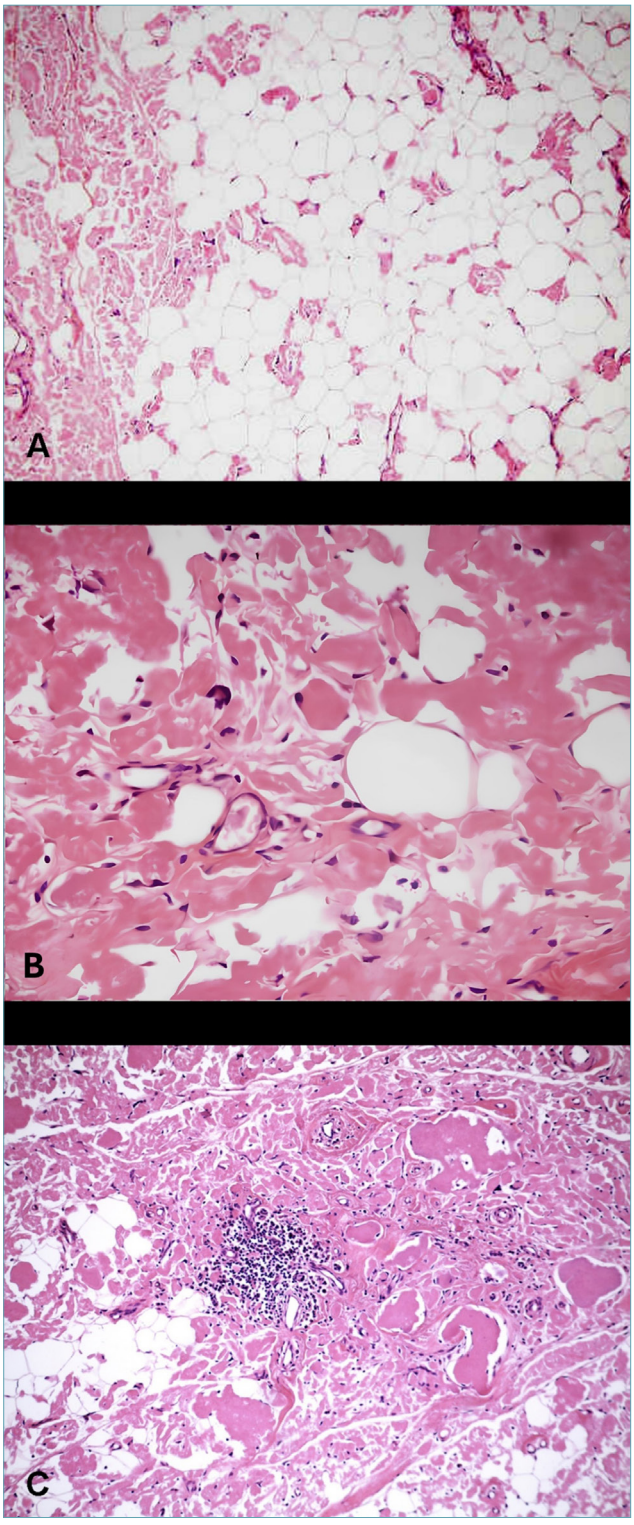

Figure 3. Amyloidoma of soft tissues. Amyloid deposits are distributed mainly between the adipocytes of the subcutaneous fat (A) (H&E, 2.5X). Several "atypical" cells are present within the amyloid substance (B) (H&E, 40X), which were further characterized as CD68 positive histiocytes. Sparse aggregates of lymphocytes are present within the amyloid substance (C) (H&E, 4X).

ments. In addition, in case 1, several scattered atypical cells, both mono and multinucleated, were present within the hyaline extracellular matrix, as well as near mature adipocytes (Fig. 3A). These cells appeared as spindle elements with central hyperchromatic nucleus, or as larger polygonal cells often with two or three nuclei. This appearance mimicked quite closely that of an adipocytic neoplasm. Scattered clusters of foreign body giant cells and scant infiltrates of mature-appearing lymphocytes and plasma cells were also detected (Fig. 3B-C). The adipocytes showed moderate variation in shape and dimension, but no atypical nuclear features were observed. However, the possibility of atypical lipomatous tumor was considered in the histologic differential diagnosis, but was excluded based on a negative staining for MDM2.

In all cases, amyloid deposits were positive for Congo-red with apple-green birefringence. Immunohistochemistry showed positivity for kappa light chain in all cases except for case 1, that was negative for both kappa and lambda light chains (Tab. I). In addition, plasma cells were positive for CD138 and MUM1, whereas histiocytes and multinucleated foreign body-type giant cells were CD68 positive.

Protein identification via bottom-up proteomics

LCM of the amyloid regions, as defined by Congo Red positivity, was performed on FFPE patient tissues obtained from the four amyloidoma cases. Table II shows the size of the areas isolated by LCM, and the number of protein groups identified by LC-MS/MS.

Quantitative microproteomics analysis of the proteins extracted from the isolated amyloidoma regions led to the identification of 212 to 911 proteins groups (Supporting Material 1). The levels of the 30 most abundant proteins from each patient are shown in Figure 4. For cases 1-3 the most abundant protein was an immunoglobulin, while for case 4 keratin and hemoglobin chains were more abundant than the amylogenic protein, probably indicating ambient/blood contamination. The 30 most abundant proteins in the amyloidoma region of case 1 (Fig. 4A) included 5 immunoglobulin light chains (IGLV6-57, IGLC2, IGKV3-20, IGKC, IGKV2-40) and one heavy chain (IgG-1 heavy chain). The most

Table II. Areas isolated by LCM and number of protein groups identified in samples from cases 1-4.

Case	Isolated plaque area	# protein groups
1	0.208 mm^2	365
2	0.131 mm^2	911
3	> 0.4 mm^2	267
4	0.385 mm^2	212

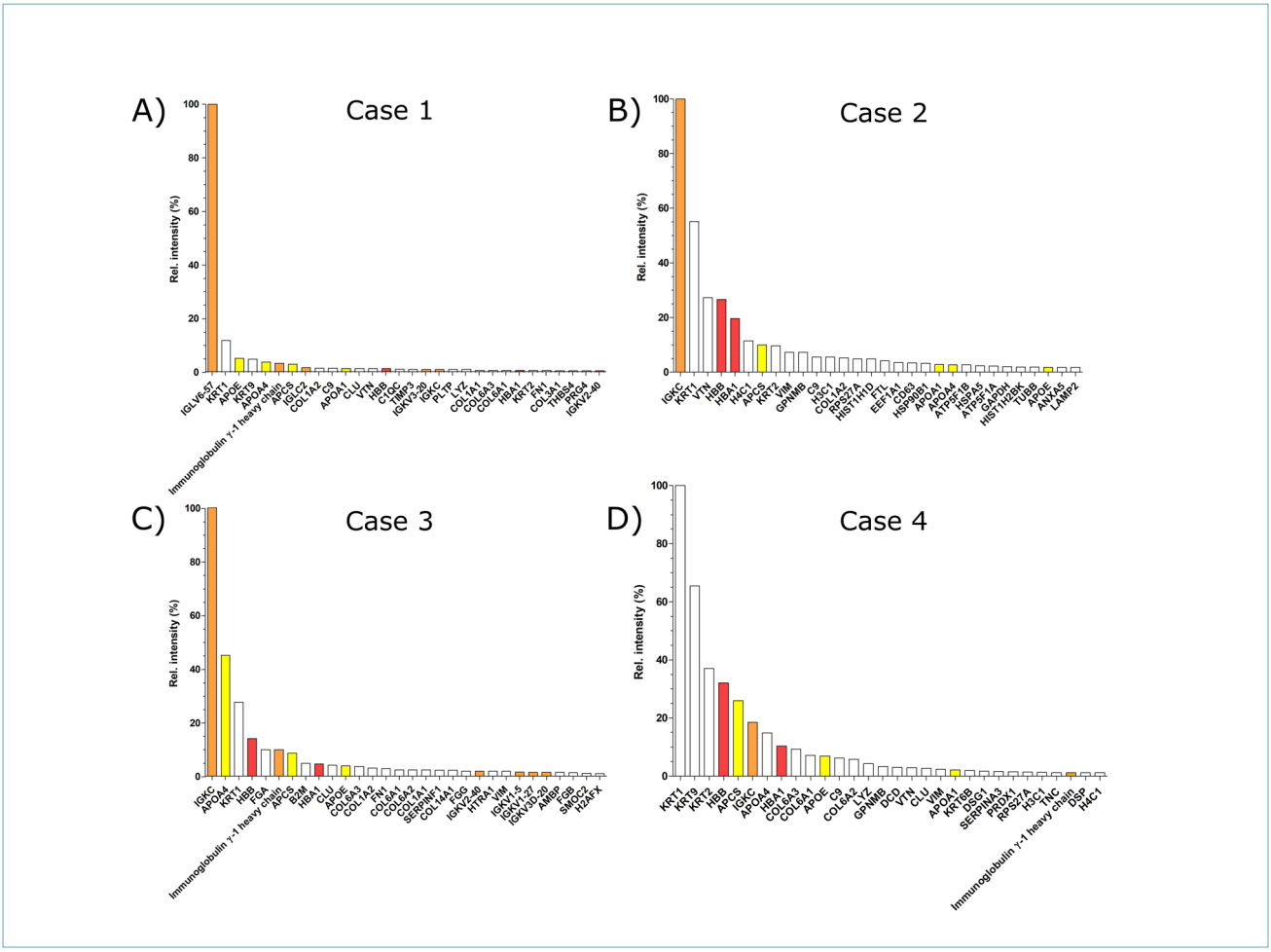

Figure 4. The 30 most abundant protein groups identified by LC-MS/MS based proteomics of the Congo-Red positive regions. Bar plots showing the relative intensity of the protein groups, with respect to the most abundant protein in the dataset, for cases 1-4 (A-D). Protein groups highlighted in orange are known to form amyloid plaques, protein groups highlighted in yellow are known to co-precipitate in the amyloid plaque. Hemoglobin chains are highlighted in red.

abundant protein group, IGLV6-57 (Immunoglobulin lambda variable 6-57), is the variable domain of the $\lambda 6$ light chain immunoglobulin [17]; its very high level indicates a local AL-lambda amyloidoma. IGLV6-57 was identified with 103 MS/MS spectra that matched to a single unique peptide, and which represents 17% sequence coverage. The second most abundant amyloid protein was the IgG-1 heavy chain, whose intensity was just 3.4% of the intensity of IGLV6-57.

For both cases 2 and 3 (Fig. 4B-C) the most abundant protein group is IGKC, the constant region of immunoglobulin κ light chains, indicating an AL-kappa amyloidoma. IGKC was identified in case 2 with 110 MS/MS spectra matching to 7 peptides (all unique), and which represented 80% sequence coverage. IGKC was identified in case 3 by 112 MS/MS spectra matching 8 peptides, all of them assigned either to IGKC chain or to immunoglobulin kappa light chain (P0DOX7), covering 84% of the protein sequence. In case 4 the most abundant amylogenic protein is IGKC, which was detected as the 6th most abundant protein in the dataset, identified through 49 MS/MS spectra matching to 7 peptides (two of which unique to the protein), representing 80% sequence coverage (Fig 4D). The plaque was thus determined to be an AL-kappa amyloidoma. The sample from patient 4 contained high levels of keratin and hemoglobin chains, indicative of contamination due to handling and blood respectively, and was presumably the reason why IGKC was only the 6th most abundant protein identified.

Discussion

Amyloidomas or amyloid tumors are nodular tumor-like masses of amyloid that may occur at various body sites, but their localization in the skeleton and soft tissues of the extremities is exceedingly rare [18]. Such tumoral deposits often lead to the suspicion of a neoplastic process, both clinically and histologically, and the diagnosis may be challenging.

In the present series, two amyloidomas arising in bone represented massive amyloid deposition associated with multiple myeloma, and one localized in the subcutaneous soft tissues of the leg was associated with Sjogren syndrome and chronic hepatic disease. In the remaining case involving the soft tissues of the popliteal fossa there was no clear evidence of systemic or chronic disease. Although rare, this occurrence has been previously reported in the literature [19]. In these cases, it has been hypothesized that the plasma cell clone may be obscured by the amyloid deposits and difficult to recognize, and amyloid deposits with no or sparse plasma cell infiltrate may indeed represent a 'burnt-out' plasmacytoma [20].

Histologically, the cases reported here show remarkable similarities to those previously described and required careful evaluation to exclude a neoplasm. Amyloid deposits that assume a tumor-like clinical presentation most often are accompanied by an intense inflammatory reaction with foreign body giant cells that may obscure the amyloid substance, necessitating a distinction from giant cell rich tumors, including tenosynovial giant cell tumor, giant cell tumor of the soft tissues, or osteoclastic giant cell-rich tumors of bone. Notably, case 1 of the present series resembled quite closely an adipocytic neoplasm both clinically and histologically. Indeed, amyloid deposits were distributed mainly between the adipocytes of the subcutaneous fat, and less prominently with a solid nodular appearance. In addition, several "atypical" cells were present within the amyloid substance, thus forming a picture that mimicked quite closely the appearance of atypical lipomatous tumor/well differentiated liposarcoma. Most of these cells were CD68 positive histiocytes, the remaining negative elements likely being fibroblasts and myofibroblasts. Atypical lipomatous tumor/well differentiated liposarcoma can be further excluded with a negative staining for MDM2 and CDK4 or with a search for the amplification of the 12q13-15 chromosome region using FISH or other molecular methods.

LCM coupled with microproteomics was used to confirm the nature of the protein deposit. A comparison of the results obtained from mass spectrometry-based typing of amyloidomas with those obtained via immunohistochemistry is shown in Table III. Cases 2-4 displayed high concordance with immunohistochemistry analysis, but case 1 could only be typed by mass spectrometry. Case 1 was determined to be an AL-lambda amyloidoma by mass spectrometry, whereas IHC was negative for both kappa and lambda chains. This result might be due to the lower sensitivity of IHC compared to LC-MS/MS based proteomics. AL is the most common amyloid deposit in systemic [21] and localized amyloidosis [22] and is generally associated with plasma cell dyscrasia or multiple myeloma [21]. The $\lambda 6$ family is overrepresented among amyloid proteins [23]; IGLV6-57 in particular is known to form amyloid fibrils [24-26]. Constant regions of light chain immunoglobulins have been shown to deposit alongside variable domains in amyloid plaques [27] and have a role in fibril aggregation [28,29]. The lack of identification of the variable domains is likely due to the somatic mutations of the variable sequences, which were not present in the FASTA database used for the database search [30]. IHC of cases 2 and 3, both determined to be AL-kappa amyloidomas by mass spectrometry, were positive for kappa chains and negative for lambda chains, fully confirming the MS-based typing. IHC of tissues from case 4 were positive for both kappa and lambda chains, whereas the MS-based analysis determined the amyloidoma type to be AL-kappa. This difference in typing may be due to the blood contamination of the sample from case 4, leading to false positive immunohistochemical positivity for AL-lambda.

Table III. Summary of MS-based and IHC-based amyloidoma typing for cases 1-4.

Case	MS-based diagnosis	Most abundant protein group	IHC-based diagnosis
1	AL-lambda	IGLV6-57	kappa-, lambda-
2	AL-kappa	IGKC	kappa+, lambda-
3	AL-kappa	IGKC	kappa+, lambda-
4	AL-kappa	IGKC	kappa+, lambda+

In general, proteomics showed concordance with IHC, and elucidated the nature of the protein deposit in the dubious IHC cases 1 and 4. Several proteins known to deposit within the amyloid plaque were also among the thirty most abundant proteins, including the "amyloid signature" [21,26,31] proteins apolipoprotein E (APOE), apolipoprotein A-IV (APOA4) and serum amyloid-P component (APSC). APOA1 is another amyloid precursor [21]; APOA1, together with APOA4, APOE and APSC, have been detected in many cases of λ light chain amyloidomas [32].

Calcification and/or ossification may occur within the amyloid produced by plasmacytomas [1,33,34]. Radiographically, these tumors present with lytic expansile

destruction of bone, often associated with an internal calcified or osseous matrix, an appearance that may simulate the appearance of chondrosarcoma [1,33]. In these cases, amyloid deposits assume the appearance of rounded bodies with a vague concentric lamination resembling corpora amylacea or undergo calcification or osseous metaplasia. To investigate possible biological pathways linked with calcification, proteins identified from case 2 (calcified femur amyloidoma) were compared with proteins from case 3 (normal appearance femur amyloidoma). Gene Ontology analysis was performed on protein identified exclusively from case 1, but no significant enrichment in bone formation or calcification-related pathways was observed (Supporting Material 2). The extremely low number of samples and the restriction of the proteomic analysis to the amyloid plaque region do not allow to draw any conclusion on the nature of the calcification detected in case 2.

In conclusion, four cases of amyloidoma were described by histopathological examination flanked by IHC and proteomics typing of the amyloid deposit. Proteomics techniques allowed to elucidate the nature of the amyloid protein deposit, improving the results obtained by immunohistochemistry. IHC results were confirmed in two cases while LCM coupled with bottom-up microproteomics was necessary to type the other two cases, for which IHC was inconclusive. Proteomic techniques were thus confirmed as a fundamental tool for the complete investigation of protein deposits.

Conflict of interest statement

The authors report there are no competing interests to declare.

Funding

This research received no external funding.

Ethiccal consideration

This study is covered by ethical vota of the medical faculty of the University of Pisa for retrospective translational research activities. An informed consent was collected from all patients. The study was approved by the ethics committee 'Comitato Etico Regionale per la Sperimentazione Clinica della Regione Toscana, Sezione: Area Vasta Nord Ovest' (protocol n. 16037). All experiments, which are routinely performed for diagnostic purposes, were performed in accordance with the principle of Good Clinical Practice (GCP) and the ethical principles contained in the current version of the Declaration of Helsinki.

Author Contributions

F.G. and R.G. performed study concept and design; F.G., F.A., and L.McD. performed development of methodology; F.G., R.G., A.F. and L.McD. performed writing, review and revision of the paper; F.G., R.G., A.F., R.C. and L.A. provided acquisition, analysis and interpretation of data. All authors read and approved the final paper.

Data availability

The data that support the findings of this study are openly available in PRIDE repository [35] at https://www.ebi.ac.uk/pride/archive, reference number PXD031789.

Abbreviations

LCM: Laser-capture microdissection
CR: Congo red
LC: liquid chromatography
MS: Mass spectrometry
ACN: acetonitrile
FA: formic acid
FFPE: formalin-fixed paraffin-embedded
Tris: tris(hydroxymethyl)aminomethane
EDTA: Ethylenediaminetetraacetic acid
SDS: Sodium dodecyl sulfate
IAA: Iodoacetamide
MeOH: Methanol
TEAB: Triethylammonium bicarbonate
LysC: Endoproteinase Lys-C
FA: formic acid
AGC: automatic gain control
LC-MS/MS: liquid chromatography-tandem mass spectrometry
PSM: peptide-spectrum match
IHC: immunohistochemistry

References

1 Pambuccian SE, Horyd ID, Cawte T, Huvos AG. Amyloidoma of Bone, A Plasma Cell/Plasmacytoid Neoplasm. Am J Surg Pathol. 1997 Feb;21(2):179-86. https://doi.org/10.1097/00000478-199702000-00007. PMID: 9042284.

2 Krishnan J, Chu W-S, Elrod JP, Frizzera G. Tumoral Presentation of Amyloidosis (Amyloidomas) in Soft Tissues: A Report of 14 Cases. Am J Clin Pathol. 1993 Aug;100(2):135-44. https://doi.org/10.1093/ajcp/100.2.135. PMID: 8356946.

3 Wechalekar AD, Gillmore JD, Hawkins PN. Systemic amyloidosis. Lancet. 2016 Jun 25;387(10038):2641-2654. https://doi.org/10.1016/S0140-6736(15)01274-X. Epub 2015 Dec 21. PMID: 26719234.

4 Dasari S, Theis JD, Vrana JA, et al. Amyloid Typing by Mass Spectrometry in Clinical Practice: a Comprehensive Review of 16,175 Samples. Mayo Clin Proc. 2020 Sep;95(9):1852-1864. https://doi.org/10.1016/j.mayocp.2020.06.029. PMID: 32861330.

5 Theis JD, Dasari S, Vrana JA, et al. Shotgun-proteomics-based clinical testing for diagnosis and classification of amyloidosis. J Mass Spectrom. 2013 Oct;48(10):1067-77. https://doi.org/10.1002/jms.3264. PMID: 24130009.

[6] Vrana JA, Gamez JD, Madden BJ, et al. Classification of amyloidosis by laser microdissection and mass spectrometry-based proteomic analysis in clinical biopsy specimens. Blood. 2009 Dec 3;114(24):4957-9. https://doi.org/10.1182/blood-2009-07-230722. Epub 2009 Oct 1. PMID: 19797517.

[7] Lavatelli F, Perlman DH, Spencer B, et al. Amyloidogenic and associated proteins in systemic amyloidosis proteome of adipose tissue. Mol Cell Proteomics. 2008 Aug;7(8):1570-83. https://doi.org/10.1074/mcp.M700545-MCP200. Epub 2008 May 12. PMID: 18474516; PMCID: PMC2494907.

[8] Brambilla F, Lavatelli F, Di Silvestre D, et al. Shotgun protein profile of human adipose tissue and its changes in relation to systemic amyloidoses. J Proteome Res. 2013 Dec 6;12(12):5642-55. https://doi.org/10.1021/pr400583h. Epub 2013 Oct 21. PMID: 24083510.

[9] Aebersold R, Mann M. Mass spectrometry-based proteomics. Nature. 2003 Mar 13;422(6928):198-207. https://doi.org/10.1038/nature01511. PMID: 12634793.

[10] Domon B, Aebersold R. Mass spectrometry and protein analysis. Science. 2006 Apr 14;312(5771):212-7. https://doi.org/10.1126/science.1124619. PMID: 16614208.

[11] Eng JK, Mccormack AL, Yates JR. An Approach to Correlate Tandem Mass Spectral Data of Peptides with Amino Acid Sequences in a Protein Database. J Am Soc Mass Spectrom. 1994 Nov;5(11):976-89. https://doi.org/10.1016/1044-0305(94)80016-2. PMID: 24226387.

[12] Steen H, Mann M. The ABC's (and XYZ's) of peptide sequencing. Nat Rev Mol Cell Biol. 2004 Sep;5(9):699-711. https://doi.org/10.1038/nrm1468. PMID: 15340378.

[13] Espina V, Wulfkuhle JD, Calvert VS, et al. Laser-capture microdissection. Nat Protoc. 2006;1(2):586-603. https://doi.org/10.1038/nprot.2006.85. PMID: 17406286.

[14] HaileMariam M, Eguez RV, Singh H, et al. S-Trap, an Ultrafast Sample-Preparation Approach for Shotgun Proteomics. J Proteome Res. 2018 Sep 7;17(9):2917-2924. https://doi.org/10.1021/acs.jproteome.8b00505. Epub 2018 Aug 28. PMID: 30114372.

[15] Heberle H, Meirelles VG, da Silva FR, et al. InteractiVenn: A web-based tool for the analysis of sets through Venn diagrams. BMC Bioinformatics. 2015 May 22;16(1):169. https://doi.org/10.1186/s12859-015-0611-3. PMID: 25994840; PMCID: PMC4455604.

[16] Szklarczyk D, Gable AL, Nastou KC, et al. The STRING database in 2021: Customizable protein-protein networks, and functional characterization of user-uploaded gene/measurement sets. Nucleic Acids Res. 2021 Jan 8;49(D1):D605-D612. https://doi.org/10.1093/nar/gkaa1074. Erratum in: Nucleic Acids Res. 2021 Oct 11;49(18):10800. PMID: 33237311; PMCID: PMC7779004.

[17] Lefranc MP. Nomenclature of the human immunoglobulin lambda (IGL) genes. Exp Clin Immunogenet. 2001;18(4):242-54. https://doi.org/10.1159/000049203. PMID: 11872955.

[18] Sidoni A, Alberti PF, Bravi S, Bucciarelli E. Amyloid tumours in the soft tissues of the legs. Case report and review of the literature. Virchows Arch. 1998 Jun;432(6):563-6. https://doi.org/10.1007/s004280050206. PMID: 9672199.

[19] Maheshwari AV, Muro-Cacho CA, Kransdorf MJ, Temple HT. Soft-tissue amyloidoma of the extremities: a case report and review of literature. Skeletal Radiol. 2009 Mar;38(3):287-92. https://doi.org/10.1007/s00256-008-0621-6. Epub 2008 Dec 3. PMID: 19050870.

[20] Westermark P. Localized AL amyloidosis: a suicidal neoplasm? Ups J Med Sci. 2012 May;117(2):244-50. https://doi.org/10.3109/03009734.2012.654861. Epub 2012 Feb 15. PMID: 22335280; PMCID: PMC3339556.

[21] Picken MM. The Pathology of Amyloidosis in Classification: A Review. Acta Haematol. 2020;143(4):322-334. https://doi.org/10.1159/000506696. Epub 2020 May 11. PMID: 32392555.

[22] Biewend ML, Menke DM, Calamia KT. The spectrum of localized amyloidosis: a case series of 20 patients and review of the literature. Amyloid. 2006 Sep;13(3):135-42. https://doi.org/10.1080/13506120600876773. PMID: 17062379.

[23] Pokkuluri PR, Solomon A, Weiss DT, et al. Tertiary structure of human lambda 6 light chains. Amyloid. 1999 Sep;6(3):165-71. https://doi.org/10.3109/13506129909007322. PMID: 10524280.

[24] Swuec P, Lavatelli F, Tasaki M, et al. Cryo-EM structure of cardiac amyloid fibrils from an immunoglobulin light chain AL amyloidosis patient. Nat Commun. 2019 Mar 20;10(1):1269. https://doi.org/10.1038/s41467-019-09133-w. PMID: 30894521; PMCID: PMC6427027.

[25] Lin Y, Marin-Argany M, Dick CJ, et al. Mesenchymal stromal cells protect human cardiomyocytes from amyloid fibril damage. Cytotherapy. 2017 Dec;19(12):1426-1437. https://doi.org/10.1016/j.jcyt.2017.08.021. Epub 2017 Oct 14. PMID: 29037943; PMCID: PMC6456258.

[26] Bhat A, Selmi C, Naguwa SM, et al. Currents concepts on the immunopathology of amyloidosis. Clin Rev Allergy Immunol. 2010 Apr;38(2-3):97-106. https://doi.org/10.1007/s12016-009-8163-9. PMID: 19626465.

[27] Blancas-Mejia LM, Misra P, Dick CJ, et al. Immunoglobulin light chain amyloid aggregation. Chem Commun (Camb). 2018 Sep 20;54(76):10664-10674. https://doi.org/10.1039/c8cc04396e. PMID: 30087961; PMCID: PMC6148388.

[28] Yamamoto K, Yagi H, Lee YH, et al. The amyloid fibrils of the constant domain of immunoglobulin light chain. FEBS Lett. 2010 Aug 4;584(15):3348-53. https://doi.org/10.1016/j.febslet.2010.06.019. Epub 2010 Jun 18. PMID: 20580354.

[29] Klimtchuk ES, Gursky O, Patel RS, et al. The critical role of the constant region in thermal stability and aggregation of amyloidogenic immunoglobulin light chain. Biochemistry. 2010 Nov 16;49(45):9848-57. https://doi.org/10.1021/bi101351c. Epub 2010 Oct 20. PMID: 20936823; PMCID: PMC4080313.

[30] Merlini G, Dispenzieri A, Sanchorawala V, et al. Systemic immunoglobulin light chain amyloidosis. Nat Rev Dis Primers. 2018 Oct 25;4(1):38. https://doi.org/10.1038/s41572-018-0034-3. PMID: 30361521.

[31] Picken MM, Herrera GA, Dogan A (edt). Amyloid and Related Disorders. Surgical Pathology and Clinical Correlations (2nd edition). New York: Humana Press, 2015.

[32] Rodriguez FJ, Gamez JD, Vrana JA, et al. Immunoglobulin derived depositions in the nervous system: Novel mass spectrometry application for protein characterization in formalin-fixed tissues. Lab Invest. 2008 Oct;88(10):1024-37. https://doi.org/10.1038/labinvest.2008.72. Epub 2008 Aug 18. PMID: 18711355.

[33] Reinus WR, Kyriakos M, Gilula LA, et al. Plasma cell tumors with calcified amyloid deposition mistaken for chondrosarcoma. Radiology. 1993 Nov;189(2):505-9. https://doi.org/10.1148/radiology.189.2.8210382. PMID: 8210382.

[34] Karasick D, Schweitzer ME, Miettinen M, O'Hara BJ. Osseous metaplasia associated with amyloid-producing plasmacytoma of bone: a report of two cases. Skeletal Radiol. 1996 Apr;25(3):263-7. https://doi.org/10.1007/s002560050076. PMID: 8741064.

[35] Vizcaíno JA, Côté RG, Csordas A, et al. The Proteomics Identifications (PRIDE) database and associated tools: Status in 2013. Nucleic Acids Res. 2013 Jan;41(Database issue):D1063-9. https://doi.org/10.1093/nar/gks1262. Epub 2012 Nov 29. PMID: 23203882; PMCID: PMC3531176.

Supporting Material

Supporting Material 1. List of identified protein groups in cases 1-4.
Supporting Material 2. List of protein groups identified exclusively in case 1, exclusively in case 2 or in common between case 1 and 2. Enrichment analysis of protein groups exclusively identified in case 1 (Cellular component and KEGG pathways).